ADVANCED FUNCTIONAL MATERIALS
www.afm-journal.de

Materials Views
www.MaterialsViews.com

An Organic Nanoparticle Transistor Behaving as a Biological Spiking Synapse

By *Fabien Alibart, Stéphane Pleutin, David Guérin, Christophe Novembre, Stéphane Lenfant, Kamal Lmimouni, Christian Gamrat,* and *Dominique Vuillaume**

Molecule-based devices are envisioned to complement silicon devices by providing new functions or by implementing existing functions at a simpler process level and lower cost, by virtue of their self-organization capabilities. Moreover, they are not bound to von Neuman architecture and this feature may open the way to other architectural paradigms. Neuromorphic electronics is one of them. Here, a device made of molecules and nanoparticles—a nanoparticle organic memory field-effect transistor (NOMFET)—that exhibits the main behavior of a biological spiking synapse is demonstrated. Facilitating and depressing synaptic behaviors can be reproduced by the NOMFET and can be programmed. The synaptic plasticity for real-time computing is evidenced and described by a simple model. These results open the way to rate-coding utilization of the NOMFET in dynamical neuromorphic computing circuits.

1. Introduction

It is now well recognized that electronic circuits based on the von Neuman paradigm are unable to catch the behavior of the complex, real-world environment, as can biological neural systems (e.g., the human brain). One of the reasons is the so-called ''von Neuman bottleneck''[1] due to the physical separation of computing units and memories. In the brain, memory and computation are mixed together and allow the processing of information both in time and space via the time-dependent properties of interconnected neurons.[1,2] This challenge for the development of a new generation of computers has induced a lot of effort in neuroscience computation activities and the framework for the spatiotemporal processing of information seems to be theoretically achievable.[2] One key element that is still a limitation concerns the integration of neurons and synaptic connections in order to realize a brain-like computer. Even though silicon CMOS (complementary metal-oxide-semiconductor) chips have been designed and fabricated to emulate the brain behaviors,[3,4] this approach is limited to small systems because it takes several (at least seven) silicon transistors to build an electronic synapse.[5] As the human brain contain more synapses than neurons (by a factor of approximately 10^7), it is essential to develop a nanoscale, low power, synapse-like device if we want to scale neuromorphic circuits towards the level of the human brain. This feature has recently prompted the research for nanoscale synaptic devices. Proposals for such programmable memory devices include optically-gated carbon-nanotube field-effect transistors (OGCNTFETs),[6,7] organic/hybrid Si nanowire transistors,[8] and memristors.[9–12]

Here, we show that mixing nanoparticles (NPs) and molecules to implement computation and memory in a single synapse-like device is a powerful approach towards such objectives. NPs and molecules are nanosize objects suitable for nanodevice fabrication; they can be manipulated and assembled by low-cost, bottom-up, techniques (e.g., self-assembly),[13,14] and are prone to work on flexible, plastic substrates (as shown by the tremendous efforts expended on plastic, printable, organic electronics).[15–17]

The nanoparticle organic memory field-effect transistor (NOMFET) demonstrated here can be programmed to work as a facilitating or depressing synapse; it exhibits short-term plasticity (STP) for dynamical processing of spikes. This behavior is obtained by virtue of the combination of two properties of the NOMFET: the transconductance gain of the transistor and the memory effect due to charges stored in the NPs. The NPs are used as nanoscale capacitors to store the electrical charges and they are embedded into an organic semiconductor (pentacene). Thus, as detailed in Section 4, the transconductance of the transistor can be dynamically tuned by the amount of charge in the NPs. We previously demonstrated that this type of device works as a memory[18] but with a ''leaky'' behavior. The retention times are in the range of a few seconds to a few thousands of seconds. This

[*] Dr. F. Alibart, Dr. S. Pleutin, Dr. D. Guérin, Dr. S. Lenfant, Dr. K. Lmimouni, Dr. D. Vuillaume
Molecular Nanostructures and Devices group
Institute for Electronics Microelectronics and Nanotechnology (IEMN)
CNRS, University of Lille
BP60069, avenue Poincaré, F-59652 cedex, Villeneuve d'Ascq (France)
E-mail: dominique.vuillaume@iemn.univ-lille1.fr
Dr. C. Novembre, Dr. C. Gamrat
CEA, LIST/LCE (Advanced Computer technologies and Architectures)
Bat. 528, F-91191, Gif-sur-Yvette (France)

DOI: 10.1002/adfm.200901335

© 2010 WILEY-VCH Verlag GmbH & Co. KGaA, Weinheim

behavior is used here to implement the synaptic weight w_{ij} with a possible dynamic working in this time range, a necessary condition to obtain the training/learning capabilities of a spiking neural network.[19] A transistor is basically a multiplier, it is used to realize the basic function of the synapse described as $S_j = w_{ij}\ S_i$, where S_i and S_j are the pre- and post-synaptic signals (here the source/drain current and voltage of the NOMFET). The synaptic weight w_{ij} is a time-dependent parameter whose value depends on the activity of the pre- and post-synapse neurons. We demonstrate that we can tailor the dynamic behavior of the NOMFET in the frequency/time domain (0.01–10 Hz) by adjusting the size of both the NPs (5–20 nm in diameter) and the size of the NOMFET (channel length L from 200 nm to 20 μm). We also demonstrate that models developed to explain and simulate the plasticity of biological synapses can be successfully adapted to the NOMFET behavior. These results open the way to the rate-coding utilization[20] of the NOMFET in neuromorphic computing circuits.[21]

2. NOMFET—Materials and Fabrication

The NOMFET (Fig. 1) consists of a bottom-gate, bottom source–drain contacts organic transistor configuration. We immobilized the gold NPs (20, 10 and 5 nm in diameter) into the source–drain channel using surface chemistry (self-assembled monolayers or SAM). They were subsequently covered by a thin film (35 nm thick) of pentacene (see the Experimental Section). This device gathers the behavior of a transistor and a memory.[18] We selected several sizes for the NPs and channel lengths of the NOMFET (200 nm to 20 μm) to study their impact on the synaptic behavior of the NOMFET. We also studied the dependence of this behavior as a function of the NP density. Figure 1 shows scanning electron microscopy (SEM) images of NP arrays with NP densities ranging from approximately 10^{10} cm^{-2} to a quasi-continuous 2D film. The density of the NP network is controlled by the density of NPs in solution and the duration of the reaction (see the Experimental Section). The optimum NP density to observe the synaptic behavior reported here is between 10^{11} and 10^{12} cm^{-2}, as shown in Figure 1b–d for the 5, 10 and 20 nm NPs, respectively. A density that is too low, $<10^{11}$ NP cm^{-2}, (Fig. 1a) leads to the memory and synaptic behaviors of the NOMFET being too weak. At high density, $>10^{12}$ NP cm^{-2}, (above the percolation threshold, such as in Fig. 1e), the device does not exhibit a transistor behavior due to metallic shorts between source and drain, and screening of the gate voltage by the metallic film of NPs.

In the following, we focus on devices with a NP density of around 10^{11} cm^{-2}. In all cases (Fig. 1b–d), we obtained a rather uniform distribution of NPs (no NP aggregation) with a density of approximately 10^{11} NP cm^{-2}. Even though we optimized the process (see the Experimental Section) to got a reproducibility (i.e., a density of about 10^{11} NP cm^{-2} without aggregation) of nearly 100% in the case of the 10 and 20 nm NPs (tested on three different fabrication runs), we observed in a few cases the formation of some aggregates (see the Supporting Information, Fig. S3). A reproducibility of only 50% is obtained for the 5 nm NPs, mainly due the lack of reproducibility in forming the thiol-terminated self-assembled monolayer (SAM) on the gate oxide (see the Experimental Section). It is noteworthy that we always observed synaptic behavior in the NOMFET, even when the arrays of NPs seem under less control (see Section 4). This feature means that the synaptic behavior of the NOMFET is very robust and defect tolerant, and this can be viewed as an important advantage for the envisioned applications in neuronal computing at the nanoscale.

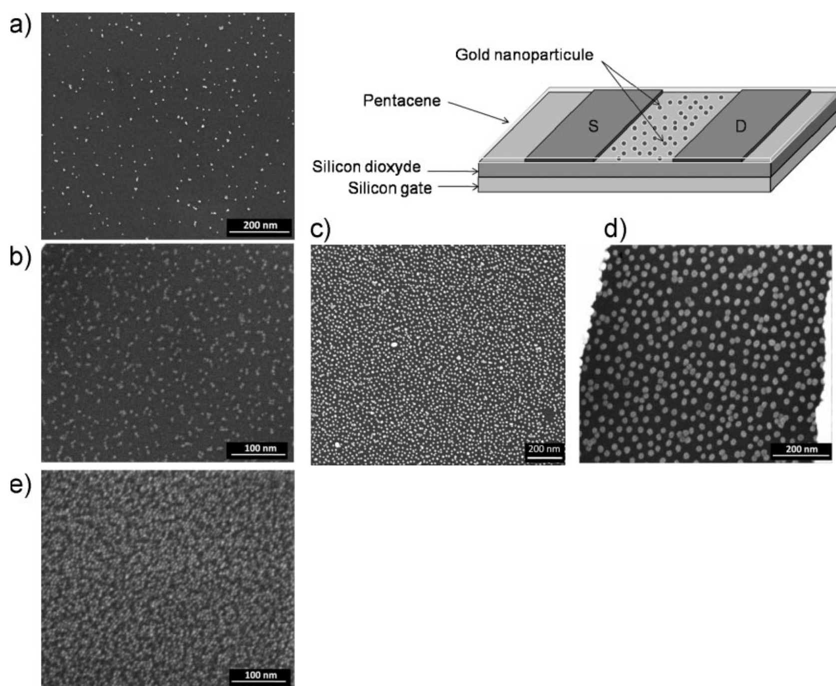

Figure 1. Scanning electron microscope image of the NP arrays before the pentacene deposition. a) 5 nm NP with a low density of 4.4×10^{10} NP cm^{-2}, b–d) 5, 10 and 20 nm NP with a medium densities of 3.7×10^{11}, 1.8×10^{11} and 0.9×10^{11} NP cm^{-2}, respectively, e) 5 nm NP with a high density $>10^{12}$ NP cm^{-2} showing a quasi 2D film with a strong percolation.

We checked, by tapping-mode atomic force microscopy (TM-AFM), the morphology of the pentacene layer deposited over the NP networks. Figure 2 shows the pentacene morphology for the reference sample (no NPs) and for the 10 nm NP NOMFET. The film without NPs shows the usual polycrystalline structure of pentacene film with large grain size and terraces, each terrace corresponding to a monolayer of pentacene molecules.[22] The pentacene film is more disordered in the presence of the NPs with a smaller grain size, and the terraces are more difficult to see. This result may be due to both the presence of NPs that hinders the surface diffusion of pentacene molecules during the deposition, and the presence of the organic SAM used to anchor the NPs on the surface. A smaller grain size has been often observed for organic field-effect transistors (OFETs) with a gate dielectric functionalized by a SAM.[23] This more-disordered pentacene film explains the decrease in the output drain current I_D and hole mobility μ_h

© 2010 WILEY-VCH Verlag GmbH & Co. KGaA, Weinheim
WILEY InterScience DISCOVER SOMETHING GREAT

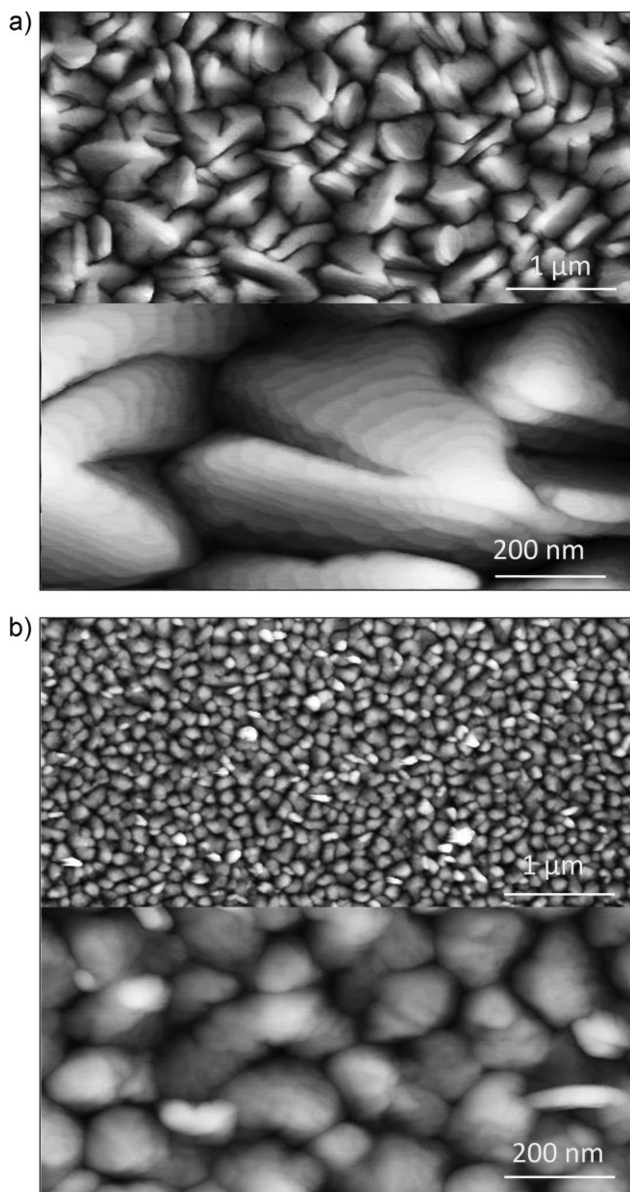

Figure 2. TM-AFM images of the 35 nm thick pentacene films at two magnifications: a) without the NPs and b) with an array of 10 nm NPs at a density of around 10^{11} NP cm^{-2}, as in Figure 1b.

measured for the NOMFET (approximately 10^{-3} cm^2 V^{-1} s^{-1}) compared to the reference device (approximately 0.1 cm^2 V^{-1} s^{-1}), as shown in Table 1. These values are averaged over 6–8 devices, and we notice that the presence of NPs induces a larger dispersion of the FET parameters. The error bars given in Table 1 are the standard deviation of a normal distribution fitted on the data; however, we did not observe a specific trend as function of the NP size.

3. Basic Behavior of a Biological Synapse

For the sake of clarity and comparison with the NOMFET, let us start with a brief description of how a biological synapse works. The most important feature of a synapse is its ability to transmit, in a given way, an action potential (AP) from one pre-synapse neuron N1, to a post-synapse neuron N2. When a sequence of APs is sent by N1 to N2, the synaptic behavior determines the way the information is treated. The synapse transforms a spike arriving from the presynaptic neuron into a chemical discharge of neurotransmitters (NTs) detected by the post-synaptic neuron and transformed into a new spike. Markram and Tsodyks[24,25] have proposed a phenomenological model to describe the synapse behavior. The synapse possesses a finite amount, U, of resources: the chemical neurotransmitters. Each spike activates a fraction aU ($a < 1$) of these resources and the amplitude I of the transmitted spike is a function of this fraction. The fraction of neurotransmitters spent to transmit the information is then recovered with a characteristic time τ_{rec} (typically in the range of a second). The response of a synapse to a train of pulses depends on the time interval between successive pulses that determines the amount of available NTs. Depending on the nature of the synapse, the response to a constant frequency train of pulses can be either depressing or facilitating (cf. Fig. 3a). Moreover, the biological synapse can process dynamical information when the frequency of the train of pulses is changed (Fig. 3b). In the case of a purely depressive synapse, a depressing behavior is obtained for a "high" frequency train of pulses (i.e., a decrease of the NTs available due to the low recovery between each spike separated by a time interval $< \tau_{rec}$), while the response of the synapse increases (facilitating behavior) at a lower frequency (the NTs get enough time to recover completely). This property has been extensively studied in biological synapses and is referred to as short-term plasticity (STP).[20,25] This simple behavior gives the synapse the main property that is necessary[2] for dynamical processing of information.

Varela et al. developed a simple iterative model[26] to simulate the STP of biological synapses. Based on the work of Magleby et al.,[27] they describe the amplitude I of a given spike in the post-synapse neuron by:

$$I = \tilde{I} F_1 \dots F_n D_1 \dots D_m \quad (1)$$

Where the F and D terms are attributed to different facilitating or depressing mechanisms with specific time constants. Thus, the

Table 1. Main transistor parameters of the NOMFET with different NP size and of the reference device (no NP). All measurements for a channel length $L = 5$ µm NOMFET. Average values and error bars correspond to the mean and standard deviation of a normal distribution fitted to the experimental data. The threshold voltage shift is the difference between the threshold voltages after and before charging the NP by a negative pulse voltage applied on the gate (−50 V for 30 s). Note that the small value measured for the reference device is known and due to traps in the pentacene or at the SiO_2/pentacene interface (see Ref. [18] and references therein).

	Average I_D [A]	Average mobility [cm^2 V^{-1} s^{-1}]	V_t shift [V]
Reference	1.8×10^{-4} ($\pm$ 8.5×10^{-5})	0.13 ($\pm$ 0.05)	1.1 ($\pm$ 0.4)
5 nm NP	2.3×10^{-6} ($\pm$ 1.6×10^{-5})	2×10^{-3} ($\pm$ 2×10^{-3})	7.5 ($\pm$ 1.4)
10 nm NP	4.1×10^{-7} ($\pm$ 7.5×10^{-7})	7.6×10^{-4} ($\pm$ 7.9×10^{-4})	9.4 ($\pm$ 0.9)
20 nm NP	3.3×10^{-7} ($\pm$ 2.8×10^{-7})	2.0×10^{-3} ($\pm$ 2.9×10^{-3})	12.8 ($\pm$ 1.8)

© 2010 WILEY-VCH Verlag GmbH & Co. KGaA, Weinheim

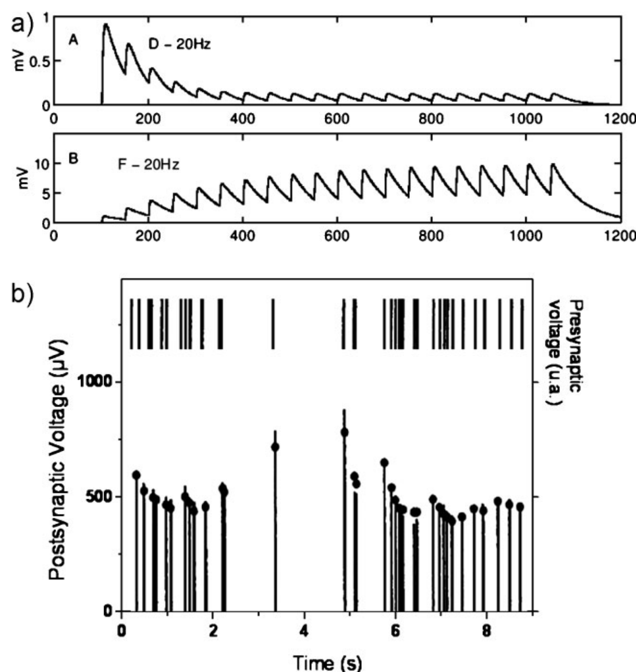

Figure 3. a) Simulation of post-synaptic potential for a depressing (top) and a facilitating (bottom) synapse submitted to the same pre-synaptic pulse train at 20 Hz (adapted from Ref. [24]). b) Comparison between the frequency-dependent post-synaptic potential response of a depressing synapse (lines) and the iterative model of Varela et al. (dots), adapted from Ref. [26], as a function of frequency of the pre-synaptic input signal.

output of the simplest depressing synapse follows $I = \tilde{I}D$, where only one depressive term is considered (this expression is also used by Abbott et al.[20]). $\tilde{I}$ is the intrinsic spike intensity delivered by the synapse (i.e., the intensity of the first spike after a long period of rest) and D is a dynamical factor representing the depression ($0 < D < 1$). The response of a synapse to a train of pulses at variable frequency is calculated by an iterative model: at each pulse arriving to the input, the output is calculated by combining the depression factor D and the amount of NTs recovered (with a time constant τ_{rec}) between two successive pulses. This quantitative model has shown a good agreement with biological synapse behavior. Figure 3b shows the comparison between the biological synapse response and the iterative model of Varela et al. with one facilitating and two depressing contributions (from Ref. [26]). We now demonstrate how the NOMFET can mimic these typical synapse behaviors.

4. NOMFET-Device Behavior Results and Synapse Analogy

We first express the NOMFET output current taking into account the effect of the charged NPs. The pentacene being a p-type semiconductor, the NOMFET is active for negative gate voltage only. Such voltage has two effects: i) As for standard transistors, it creates holes in the pentacene thin film at the interface with the insulator; and, ii) It charges positively the gold particles via the organic material. Adapting the percolation theory of Vissenberg and Matters[28] for organic thin-film transistors, the drain/source current of the NOMFET is expressed as (see the Supporting Information):

$$I_{DS} = GV_{DS} \quad with \quad G = A_0 e^{\beta \varepsilon_F} e^{-\beta \Delta} \tag{2}$$

Where G is the channel conductance, $\beta = 1/k_B\Theta$, Θ the temperature, A_0 a temperature-dependent parameter, ε_F the Fermi energy fixed by the gate voltage and Δ the shift of the Fermi energy induced by the charged NPs. The last term is caused by the repulsive electrostatic interaction between the holes trapped in the NPs and the ones in the pentacene. The effect of the positively charged NPs is to reduce the current. As an analogy with the biological synapses, the holes play the role of the neurotransmitters. They modify the output signal, I_{DS}, in a way that depends on the numbers of trapped charges via the Δ term: the more charges stored in the NPs, the more the current is reduced. Note that with electrons trapped in the NPs, the result is the opposite: the charges then increase the Fermi energy and the current. These behaviors correspond to our experimental observations, as reported elsewhere.[18] Charging NPs with holes by applying a negative voltage pulse on the gate induces a negative threshold voltage shift as measured on the drain current–gate voltage (I_D–V_G) curves of the NOMFET, and (at fixed V_D and V_G), a decrease in the current. A positive gate voltage pulse shifts the NOMFET characteristics backward.[18] From these threshold voltage shifts (Table 1) and for the optimized NOMFET with a NP density of around $10^{11}\,cm^{-2}$ (such as those shown in Fig. 1b–d), we estimated the number of charge per NP (for a gate voltage pulse of -50 V during 30 s, measured on a 5 μm channel length NOMFET at $V_D = -30$ V). They are typically approximately 2, 6 and 15 holes per NP for the 5, 10 and 20 nm NP NOMFETs, respectively.

Using these properties, we can mimic the different behaviors of the biological synapses by initially charging the NPs with holes (negative gate voltage) or discharging the NPs (positive gate voltage) depending whether we want a depressing or a facilitating behavior, respectively, before measuring the response of the NOMFET to a train of spikes. The input signal is the drain–source voltage, the output is the drain/source current (the transistor is used in a pass-transistor configuration, source and drain are reversible). The gate has two functions. In a first phase (see a chronogram of the signals in the Supporting Information, Fig. S2), we used it to program the NOMFET by applying a gate voltage pulse V_P while source and drain were grounded, and during the working phase, we applied a dc voltage V_G to maintain the transistor in its "on" regime while an input spiking voltage (between V_{D1} and V_{D2}) was applied on the drain. Figure 4a and b demonstrate that the facilitating and depressing behaviors are obtained on the same NOMFET, for rigorously the same application of pulses at the input, by initially programming the device with the gate signal V_P. For the depressing case (Fig. 4a), we applied $V_P > 0$ before running the device, while for the facilitating case $V_P < 0$ (Fig. 4b). In a biological synapse, the facilitating behavior means that an incoming signal with a given frequency and duty cycle induces a post-synaptic signal having an increasing trend, whereas in the case of a depressing synapse, the post-synaptic signal tends to decrease, as shown in Fig. 3a. We demonstrated in Figure 4 exactly the same behavior for the NOMFET, where the programming

© 2010 WILEY-VCH Verlag GmbH & Co. KGaA, Weinheim
WILEY InterScience® DISCOVER SOMETHING GREAT

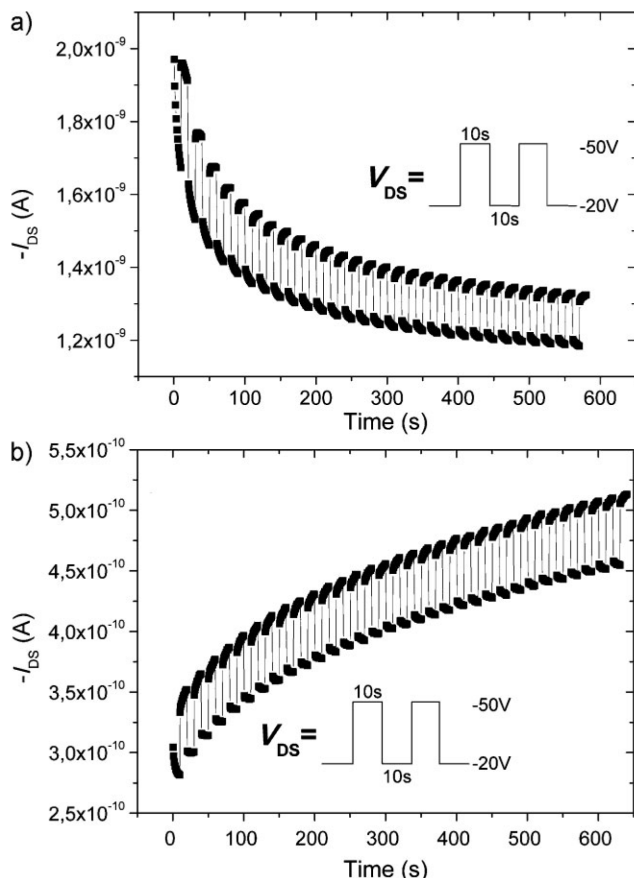

Figure 4. a) Response (drain current) of the NOMFET (5 nm NP, $L/W = 12\,\mu m/113\,\mu m$) to a constant frequency (0.05 Hz) train of pulses ($V_{D1} = -20$ V, $V_{D2} = -50$ V) after programming the device by a $V_P = 50$ V (40 s) gate pulse to discharge the NPs. The decreasing trend of the output current (in absolute value) mimics a depressing biological synapse. b) Response (drain current) of the NOMFET (5 nm NP, $L/W = 12\,\mu m/113\,\mu m$) to a constant frequency (0.05 Hz) train of pulses ($V_{D1} = -20$ V, $V_{D2} = -50$ V) after programming the device by a $V_P = -50$ V (40 s) gate pulse to charge the NPs. The increasing trend of the output current (in absolute value) mimics a facilitating biological synapse.

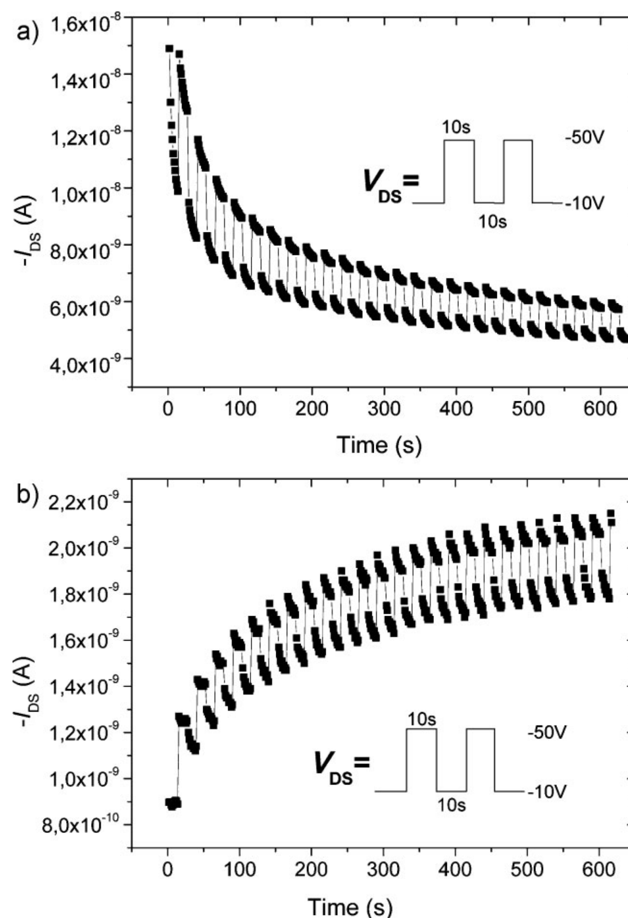

Figure 5. a) Response (drain current) of the NOMFET (20 nm NP, $L/W = 12\,\mu m/113\,\mu m$) to a constant frequency (0.05 Hz) train of pulses ($V_{D1} = -10$ V, $V_{D2} = -50$ V) after programming the device by a $V_P = 50$ V (20 s) gate pulse to discharge the NPs. The decreasing trend of the output current (in absolute value) mimics a depressing biological synapse. b) Response (drain current) of the NOMFET (20 nm NP, $L/W = 12\,\mu m/113\,\mu m$) to a constant frequency (0.05 Hz) train of pulses ($V_{D1} = -10$ V, $V_{D2} = -50$ V) after programming the device by a $V_P = -50$ V (20 s) gate pulse to charge the NPs. The increasing trend of the output current (in absolute value) mimics a facilitating biological synapse.

negative or positive gate voltage pulses induce facilitating or depressing behavior, respectively. Interestingly, the same behavior (Fig. 5) is also obtained for NOMFET with a less-controlled deposition of NPs (i.e., NPs forming aggregates, Fig. S3 in the Supporting Information). This result means that the synaptic behavior of the NOMFET is robust against process variations.

More importantly, we can reproduce the STP behavior without initial programming. We used the NOMFET as a ''pseudo-two-terminal device''. The gate receives the same input voltage (a train of pulses at frequency $1/T$, where T is the period, and amplitude V_P) as the drain/source electrode (see the Supporting Information, Fig. S2). We measured the response of the NOMFET to sequences of pulses with different periods, T (Fig. 6). During such experiments, the NPs are alternately charged during the pulse time and discharged between pulses.[18] The value of the current at a certain time (i.e., after a certain number of spikes) depends on the past history of the device, which determines the amount of charge presents in the NPs. To illustrate this point, let us consider the NOMFET ($L = 12\,\mu m$, 5 nm NPs) at the beginning of a particular sequence with period T (Fig. 6a), where the NPs contain some charges. If $T << \tau_d$ (τ_d is the NP discharge time constant, of about 20 s here; see below), more and more holes are trapped in NPs and the NOMFET presents a depressing behavior, as observed for the 0.5 and 2 Hz spike sequences. As expected, the depressing behavior is more pronounced when increasing the frequency. This result is also in good agreement with the behavior of a spiking biological synapse (see the Supporting Information). Then, for a larger period T (0.05 Hz signal in Fig. 6a), the NPs have enough time to be discharged between pulses and the sequence presents a facilitating behavior. This feature exactly reproduces the behavior of a biological synapse (Fig. 3b). The holes trapped in the NPs play the role of the neurotransmitters and the output signal, I_{DS}, is a decreasing function of the number of holes stored in the NPs[18] (Fig. 6). At each spike, a certain number of holes are trapped in the

© 2010 WILEY-VCH Verlag GmbH & Co. KGaA, Weinheim

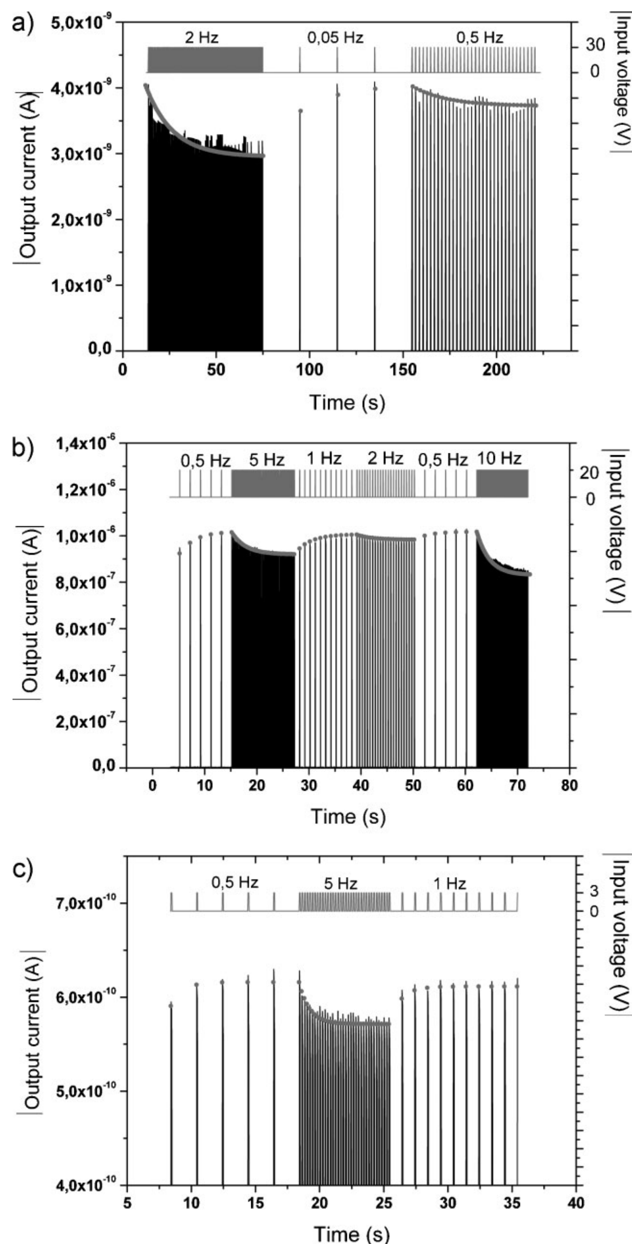

Figure 6. a) Response (drain current) of NOMFET with L/W ratio of 12 μm/113 μm and NP size of 5 nm to sequences of spikes at different frequencies (pulse voltage $V_P = -30$ V). b) Response of NOMFET with L/W ratio of 2 μm/1 000 μm and NP size of 5 nm (pulse voltage $V_P = -20$ V). c) Response of NOMFET with L/W ratio of 200 nm/1 000 μm and NP size of 5 nm (pulse voltage $V_P = -3$ V). In all cases, the grey circles correspond to the iterative model calculation (see text), the black lines are the output current measurements. Increasing the frequency evidences a depressing behavior and a facilitating one is observed by decreasing the frequency.

NPs. Between pulses the system relaxes: the holes escape with a characteristic time τ_d. We did not observe such a synaptic behavior for the reference pentacene OFET (no NPs; see the Supporting Information, Fig. S4).

Based on Equation 2 for the output current, we adapted the simplest iterative model of Varela et al.[26] to simulate the dynamical behavior of the NOMFET, and we developed an analogous modelisation. A pulse induces positive charges in the NPs: the NOMFET channel conductance is then reduces by a multiplicative factor $K < 1$. Between each pulse, the NPs tend to discharge with a characteristic time τ_d. The general equation describing the iterative model is (see supporting information):

$$I_{n+1} = I_n K e^{-(T-P)/\tau_d} + \tilde{I}\left(1 - e^{-(T-P)/\tau_d}\right) K \tag{3}$$

Where I_{n+1} and I_n are the current of the NOMFET at the end of the $(n+1)^{\text{th}}$ and n^{th} voltage pulses sent to the NOMFET, $\tilde{I}$ is the intrinsic drain current of the NOMFET, i.e., the current that the device would have if the charges in the NPs were kept in the equilibrium configuration (i.e., after a long period of rest, with no charge, or with a constant residual charge induced by the static dc bias of the device), T is the period between two pulses and P is the width of the pulses.

We fitted the iterative model to simulate the NOMFET behavior (gray dots in Fig. 6). The same fitted parameters, $\tilde{I}$ and K, and τ_d (here 4.1×10^{-9} A, 0.9 and 20 s, respectively) are used in the three successive sequences shown in Figure 6a, proving a good agreement between the model and the experiments. For instance, let us consider the system at the beginning of a particular sequence with period T ($T = 0.5$ s or $F = 2$ Hz in Fig. 6a), where the NPs contain some charges. Since $T << \tau_d$, the first term of the iterative function, $I_n K e^{-(T-P)/\tau_d}$, is the most important one and the sequence of spikes present a depressing behavior ($I_{n+1} < I_n$). On the other hand, for a larger period T ($T = 20$ s, $F = 0.05$ Hz), the second term $\tilde{I}(1 - e^{-(T-P)/\tau_d})K$ becomes the larger one and the sequence presents a facilitating behavior ($I_{n+1} > I_n$). Again, the depressing behavior for $T = 2$ s ($F = 0.5$ Hz) is well reproduced by the model.

We applied this model to different NOMFET with various W/L ratios (where L is the distance between electrodes and W the width of the electrodes) down to $L = 200$ nm. For instance, the fits shown in Figure 6b for the $L = 2$ μm NOMEFT correspond to $\tau_d = 3$ s ($\tilde{I} = 10^{-6}$ A, $K = 0.99$) and for the $L = 200$ nm NOMFET (Fig. 6c) to $\tau_d = 0.9$ s ($\tilde{I} = 6.3 \times 10^{-10}$ A, $K = 0.98$). We report in Figure 7 the evolution of τ_d with the channel length and size of the NPs. For comparison, we also plot (for some devices) the time constant extracted from basic charge/discharge measurements (see the Supporting Information, Fig. S5). We note that: i) the characteristic time from the fitted model and the direct discharge measurement are of the same order of magnitude, ii) the characteristic time, and thus the working frequency range of the NOMFET, can be adjusted by changing the channel length L of the NOMFET, and, iii) τ_d is weakly dependent on the NP size. The RC charge/discharge time constant is roughly governed by the channel resistance R of the NOMFET, which scales as L, and the self-capacitance of a NP $C_{self} = 2\pi\varepsilon D$, which scale as the NP diameter D (ε is the dielectric constant), thus scaling down L and D should, in principle, decrease τ_d. This feature is clearly observed for L.

At the macroscopic scale, we have to take into account the total capacitance, which is NC_{self} with N being the number of NPs in the channel. This number, while controlled to be around 10^{11} NP cm^{-2} (see Fig. 1), varies from device to device, and we believe that these dispersions can hinder the intrinsic role of the NP size. Moreover, the NPs are capped with surfactant molecules (see the

© 2010 WILEY-VCH Verlag GmbH & Co. KGaA, Weinheim

WILEY InterScience DISCOVER SOMETHING GREAT

FULL PAPER

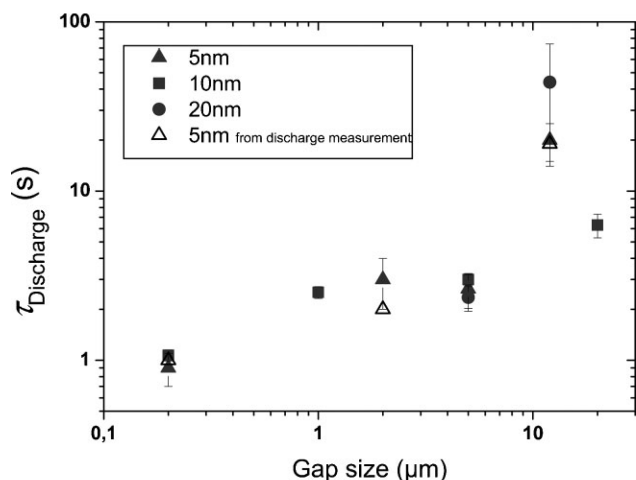

Figure 7. Evolution of the NP discharge time constant as function of the NOMFET channel length and for the different sizes of NP. Full symbols are from data extracted by fitting the model on the experiments (as in Fig. 6), open symbols are from discharge experiments (see the Supporting Information, Fig. S5).

Experimental Section), which can act as a tunnel barrier between the NPs and the pentacene. It is likely that this tunnel barrier play a role in the discharge phenomena (a thicker tunnel barrier will increase the discharge time constant). We did not control the structural quality of this tunnel barrier, which can represent an additional source of dispersion. More detailed experiments, for instance by systematically varying the length of the alkanethiol capping the NPs, will be necessary to increase the control of the charging/discharging phenomena in the NOMFET. A more accurate description of the relationship between these time constants, the size of the NPs and geometry of the NOMFET would require a more sophisticated modelization using a 2D network of distributed RC time constants (taken into account statistical dispersion) rather than a single macroscopic one.

Finally, we note that the iterative model used here to fit the experimental data can be implemented in usual device simulator (SPICE-like) allowing a reliable conception and simulation of hybrid NOMFET/CMOS neuronal circuits.[29] These device/circuit simulations can easily take into account the experimental dispersion of the NOMFET performances to test the robustness of these neuronal circuits against the actual device variation. Recently, a simple associative memory was built using a purely CMOS-based emulator of memristor (acting as the synapse) and neurone.[30] In this work, the memristor-synapse is emulated using a combination of CMOS analog-to-digital converter and microcontroller. It is likely that the NOMFET can be used as the synapse in such associative memory architecture. Such hybrid NOMFET/CMOS neuromorphic computing circuits and architectures are currently under investigation in our laboratory. At this stage, an interesting question can be raised: whether the NOMFET is more related to a memristor device[9] or more related to a memcapacitor as defined by Di Ventra et al. [31] While a definitive answer would probably require more experiments and simulations of the NOMFET, we believe that the NOMFET is more related to a charge-controlled memristor (or charge-controlled memconductance) as defined in Ref. [31], since the channel conductance of the NOMFET is history-dependent of the amount of charges stored in the NPs.

5. Conclusions

We demonstrated a hybrid nanoparticle-organic device, a NOMFET, that makes use of the charge storage capability of the nanoparticles and the amplification factor of the organic transistor to mimic the short-term plasticity of a biological synapse. The NOMFET can be programmed to exhibit either a facilitating or a depressing behavior. By adjusting the size of the device down to 200 nm and the diameter of the nanoparticle down to 5 nm, we can range the working frequency between 0.01 and 10 Hz. We simulated the synapse behavior of the NOMFET by adapting a model developed for the biological synapse. Varela et al.[26] describe the output of biological synapses as a product of several depression (*D*-terms) and facilitation (*F*-terms) factors (Eq. 1), each of these factors being associated with a particular characteristic time. For the NOMFET, by approximating the relaxation function of the NP discharge by a simple exponential, we get the simplest model of this type: our NOMFET behaves within this approximation as the simplest depressive synapse with only one *D*-term.

6. Experimental

Fabrication of Devices: The NOMFETs were processed using a bottom-gate electrode configuration. We used highly-doped ($\rho = 10^{-3}\,\Omega$ Cm) p-type silicon covered with a thermally grown 200 nm thick silicon dioxide. Before use, these wafers were cleaned by sonication in chloroform for 5 min then by a piranha solution (H_2SO_4 /H_2O_2, 2:1 v/v) for 15 min and then by ultraviolet irradiation in an ozone atmosphere (ozonolysis) for 30 min (*caution: preparation of the piranha solution is highly exothermic and it reacts violently with organics*). Electrodes (titanium/gold, 20/200 nm) were deposited on the substrate by vacuum evaporation and patterned by optical lithography (for channel length *L* between 1 and 20 µm). Smaller NOMFETs ($L = 0.2$ µm) were fabricated on thinner oxide (10 nm thick) by usual electron-beam lithography.

The SiO_2 (gate dielectric) was then functionalized as a self-assembled monolayer (SAM) to anchor gold nanoparticles (NPs) on the surface. For the largest NPs (20 and 10 nm in diameter), the SiO_2 surface was functionalized by an amino-terminated SAM before the NP deposition [13,32,33]. First, gold (Au) electrodes were functionalized by dipping in a 2-amino ethanethiol solution in ethanol (10 mg mL^{-1}) for 5 h. The sample was then rinsed 3 times with isopropanol and subsequently dried in argon stream. Second, the SiO_2 surface was functionalized by immersion in a solution of (3-aminopropyl) trimethoxysilane (APTMS) molecules (supplied by ABCR) diluted in anhydrous toluene at a concentration 1.25 µL mL^{-1} and at 60 °C for 4 min [34]. The reaction took place in a glove-box with a controlled atmosphere (nitrogen, with less than 1 ppm of oxygen and water vapor). Excess, non-reacted, molecules were removed by rinsing with toluene, and then in isopropanol under sonication. This sample was subsequently dried under an argon stream. The static water contact angle was 19°, a common value for hydrophilic NH_2-terminated surfaces [34]. This sample was then dipped in an aqueous solution of citrate-stabilized Au-NP (colloidal solution purchased from Sigma Aldrich, 20 ± 3 nm and 10 ± 3 nm diameter) overnight under an argon atmosphere. The NP concentration in the solution and duration of the reaction were changed to adjust the NP density on the surface. The sample was then cleaned with deionized water and isopropanol, and dried under argon stream. Finally, Au-NPs were encapsulated by dipping in a solution of 1,8-octanedithiol (from Aldrich) in ethanol (10 µL mL^{-1}) for 5 h to help the

© 2010 WILEY-VCH Verlag GmbH & Co. KGaA, Weinheim

formation of a network of NPs. The sample was subsequently rinsed in alcohol and dried in argon stream. For the smallest NPs, we used a solution of 4–5 nm diameter dodecanethiol-functionalized gold nanoparticles (2% in toluene) supplied by Aldrich. The oxidized silicon with gold electrodes wafer was placed overnight in the presence of vapors of freshly distilled mercaptopropyltrimethoxysilane (MPTS) in laboratory glassware at 0.2 Torr [35,36]. This freshly prepared substrate was immersed in a gold nanoparticles (NPs) solution. The starting solution supplied by Aldrich was diluted 100 times in toluene. Again, NP concentration in the solution and duration of the reaction were changed to adjust the NP density on the surface. As expected, thiol capped Au NPs readily reacted with thiol-terminated SAM by ligand exchange forming a covalent bond with the surface.

Finally, a 35 nm thick pentacene film was evaporated at a rate of 0.1 Å s^{-1}. The substrate was kept at room temperature. A reference device of pentacene without NPs (and without SAM) was also realized in the same run of deposition to evidence the effect of NPs on the electrical properties. Note that a second reference sample with a SAM between the SiO_2 and the pentacene film did not show any memory effect [37].

Electrical Measurements: The NOMFET electrical characteristics were measured with an Agilent 4155C semiconductor parameter analyzer, the input pulses were delivered by a pulse generator (Tabor 5061). The electrodes of the NOMFET were contacted with a micro-manipulator probe station (Suss Microtec PM-5) placed inside a glove box (MBRAUN) with a strictly controlled nitrogen ambient (less than 1 ppm of water vapor and oxygen). Such a dry and clean atmosphere is required to avoid any degradation of the organics (SAMs and pentacene). So the devices are not exposed to air from the beginning of the fabrication process to the end of the electrical characterization.

Acknowledgements

This work was funded by the European Union through the FP7 Project NABAB (Contract FP7-216777) and partly by the Micro and Nanotechnology Program from the French Ministry of Research under the grant RTB: "Post CMOS moléculaire". We thank R. Baptist (CEA-LETI) for his support. Supporting Information is available online from Wiley InterScience or from the corresponding author.

Received: July 20, 2009
Revised: October 5, 2009
Published online: December 16, 2009

[1] J. Backus, *Commun. ACM* **1978**, *21*, 613.
[2] D. V. Buonomano, W. Maass, *Nat. Rev. Neurosci.* **2009**, *10*, 113.
[3] G. Le Masson, S. Renaud-Le Masson, D. Debay, T. Bal, *Nature* **2002**, *417*, 854.
[4] FACETS: Fast Analog Computing with Emergent Transient States, http://facets.kip.uni-heidelberg.de (accessed October 2009).
[5] M. Boegerhausen, P. Suter, S.-C. Liu, *Neural Comput.* **2003**, *15*, 331.
[6] J. Borghetti, V. Derycke, S. Lenfant, P. Chenevier, A. Filoramo, M. Goffman, D. Vuillaume, J. P. Bourgoin, *Adv. Mater.* **2006**, *18*, 2535.
[7] G. Agnus, W. Zhao, V. Derycke, A. Filoramo, Y. Lhuillier, S. Lenfant, D. Vuillaume, C. Gamrat, J.-P. Bourgoin, *Adv. Mater.* **2009**, in press.
[8] Q. Lai, Z. Li, L. Zhang, X. Li, W. F. Stickle, Z. Zhu, Z. Gu, T. I. Kamins, R. S. Williams, Y. Chen, *Nano Lett.* **2008**, *8*, 876.
[9] D. B. Strukov, G. S. Snider, D. R. Stewart, R. S. Williams, *Nature* **2008**, *453*, 80.
[10] J. J. Yang, M. D. Pickett, X. Li, A. A. OhlbergDouglas, D. R. Stewart, R. S. Williams, *Nat. Nanotechnol.* **2008**, *3*, 429.
[11] J. Borghetti, Z. Li, J. Straznicky, X. Li, D. A. A. Ohlberg, W. Wu, D. R. Stewart, R. S. Williams, *Proc. Natl. Acad. Sci. USA* **2009**, *106*, 1699.
[12] G. S. Snider, in *IEEE/ACM International Symposium in Nanoscale Architectures* **2008**, 85.
[13] M.-C. Daniel, D. Astruc, *Chem. Rev.* **2004**, *104*, 293.
[14] W. Lu, C. M. Lieber, *Nat. Mater.* **2007**, *6*, 841.
[15] M. F. Sybille Allard, B. Souharce, H. Thiem, U. Scherf, *Angew. Chem. Int. Ed.* **2008**, *47*, 4070.
[16] H. Yan, Z. Chen, Y. Zheng, C. Newman, J. R. Quinn, F. Dotz, M. Kastler, A. Facchetti, *Nature* **2009**, *457*, 679.
[17] J. H. Cho, J. Lee, Y. Xia, B. Kim, Y. He, M. J. Renn, T. P. Lodge, C. Daniel Frisbie, *Nat. Mater.* **2008**, *7*, 900.
[18] C. Novembre, D. Guérin, K. Lmimouni, C. Gamrat, D. Vuillaume, *Appl. Phys. Lett.* **2008**, *92*, 103314.
[19] S. Haykin, *Neural Networks. A Comprehensive Foundation*, Macmillian, New York **1994**.
[20] L. F. Abbott, J. A. Varela, K. Sen, S. B. Nelson, *Science* **1997**, *275*, 220.
[21] J. J. Hopfield, *Proc. Natl. Acad. Sci. USA* **1982**, *79*, 2554.
[22] C. D. Dimitrakopoulos, D. J. Mascaro, *IBM. J. Res. & Dev.* **2001**, *45*, 11.
[23] M. Shtein, J. Mapel, J. B. Benziger, S. R. Forrest, *Appl. Phys. Lett.* **2002**, *81*, 268.
[24] M. Tsodyks, K. Pawelzik, H. Markram, *Neural Computation* **1998**, *10*, 821.
[25] M. V. Tsodyks, H. Markram, *Proc. Natl. Acad. Sci. USA* **1997**, *94*, 719.
[26] J. A. Varela, K. Sen, J. Gibson, J. Fost, L. F. Abbott, S. B. Nelson, *J. Neurosci.* **1997**, *17*, 7926.
[27] K. L. Magleby, J. E. Zengel, *J. Gen. Physiol.* **1982**, *80*, 613.
[28] M. C. J. M. Vissenberg, M. Matters, *Phys. Rev. B* **1998**, *57*, 12964.
[29] O. Bichler, W. Zhao, F. Alibart, S. Pleutin, D. Vuillaume, C. Gamrat, unpublished.
[30] Y. V. Pershin, M. di Ventra, *arXiv:cond-mat/0905.2935* **2009**.
[31] M. di Ventra, Y. V. Pershin, L. O. Chua, *Proc. IEEE* **2009**, *97*, 1717.
[32] H. X. He, D. Zhang, Q. G. Li, T. Zhu, S. F. Y. Li, Z. F. Liu, *Langmuir* **2000**, *16*, 3846.
[33] T. Sato, H. Ahmed, D. Brown, B. F. G. Johnson, *J. Appl. Phys.* **1997**, *82*, 696.
[34] D. F. Siqueira Petri, G. Wenz, P. Schunk, T. Schimmel, *Langmuir* **1999**, *15*, 4520.
[35] J. J. Senkevitch, C. J. Mitchell, G.-R. Yang, T.-M. Lu, *Langmuir* **2002**, *18*, 1587.
[36] D. K. Aswal, S. Lenfant, D. Guerin, J. V. Yakhmi, D. Vuillaume, *Small* **2005**, *1*, 725.
[37] M. Ternisien, *PhD Thesis*, University of Lille **2008**.

© 2010 WILEY-VCH Verlag GmbH & Co. KGaA, Weinheim
WILEY InterScience® DISCOVER SOMETHING GREAT